NIH Public Access
Author Manuscript
Magn Reson Med. Author manuscript; available in PMC 2008 May 26.

Published in final edited form as:
Magn Reson Med. 1988 March ; 6(3): 314–333.

Optimization of MR Protocols:

A Statistical Decision Analysis Approach

Elliot R. McVeigh, **Michael J. Bronskill**, and **R. Mark Henkelman**
Department of Medical Biophysics, University of Toronto, and Physics Division, Ontario Cancer Institute, 500 Sherbourne Street, Toronto, Ontario M4X 1K9, Canada

Abstract

A new method of optimizing MRI data acquisition protocols is presented. Tissues are modeled with probability density functions (PDFs) of tissue parameter values (such as T_1, T_2). The imaging data acquisition process is modeled as a mapping from a tissue parameter space to a signal strength space. Tissue parameter PDFs are mapped to signal strength PDFs for each tissue in a clinical problem. The efficacy of an MRI protocol is evaluated using the methods of statistical decision analysis applied to the signal strength PDFs, including the propagation of noise. This procedure evaluates the ability to discriminate different tissues based on the signal strengths produced with the protocol. The model can incorporate an arbitrary number of tissues, parameters, and pulse sequences in the protocol. The multivariate nature of MRI and the observed broad distribution of tissue parameter values makes this model more appropriate for optimizing data acquisition protocols than methods which maximize the signal-difference-to-noise ratio between discrete values of the tissue parameters. It is shown that these two methods may calculate different optimal protocols. The method can be used to optimize data acquisition for quantitative computer-based tissue classification, as well as imaging. Data acquisition and image processing philosophies are discussed in light of the method.

1. Introduction

The application of NMR in medicine, as originally proposed, was a simple diagnostic test based on measured relaxation times T_1 and T_2 (1). It was recognized that this test would be most useful when performed *in vivo* on an isolated region of tissue. Magnetic resonance imaging (MRI) techniques provided the means for this isolation and today yield tomograms of impressive visual quality. However, with the movement toward a rich radiological technique, MRI has suffered the loss of its development as a quantitative diagnostic test. The majority of the MRI research to date has been geared toward producing aesthetically pleasing images with higher signal-to-noise ratio (SNR), finer resolution, and faster scan times. While these are laudable goals in the context of imaging, it is not clear how to transform improvements in these attributes into improvements in diagnostic performance. Although many diagnoses can be made from observation of abnormal morphology, MRI offers a unique opportunity to derive a multivariate diagnostic test based on tissue parameters. In order to exploit this opportunity, we should think of the MRI experiment not as something that generates contrast between tissues, but as a process that discriminates between different tissues. This difference may seem subtle but, as this paper will show, these two philosophies lead to different methods of optimization.

Early methods for deriving optimal MRI pulse sequences applied differential calculus to the signal strength equations (2-7) and used the maximum signal-difference-to-noise ratio (SDNR) or maximum signal gradient as the quantitative figure of merit. These methods address the one-dimensional problem of producing a gray-scale representation of an object with the maximum "sensitivity" at a *specific value*, or maximum SDNR between two *specific values* of the tissue parameters; as such, they are elegant and the mathematics is straightforward. However, these methods do not directly address the problem of maximizing the sensitivity and specificity of MRI as a diagnostic test applied to a patient population. To do this, one must incorporate into

NIH-PA Author Manuscript
NIH-PA Author Manuscript
NIH-PA Author Manuscript

NIH-PA Author Manuscript

NIH-PA Author Manuscript

NIH-PA Author Manuscript

the figure of merit the ideas associated with evaluation of a diagnostic test: the reduction of multiparametric collected data into a single test value, and the distribution of expected test values from the patient population (8-10).

The need for a universal optimization method becomes more apparent with the development of each new MRI technique. Innovations in MRI tend to exploit additional tissue parameters, and bring with them new pulse sequence parameters. For example, fast imaging with gradient echoes is sensitive to chemical shift (δ) and magnetic susceptibility (χ_0), and the signal strength is highly dependent upon the interaction of relaxation rates and the rf flip angles (α). Thus, it introduces two new tissue parameters (δ, χ_0), and a new pulse sequence parameter (α). While new innovations are assumed to increase the power of MRI as a diagnostic test, the increased complexity necessitates a coherent method of choosing the subset of techniques to use in the limited examination time. What is needed is a framework upon which all of these techniques can be placed and evaluated in terms of their power as diagnostic tests, individually and when used in concert.

2. A Model of MRI as a Diagnostic Test

Images with an acceptable SNR are now available at a wide range of magnetic field strengths. They usually have a SNR far in excess of the minimum required to demonstrate the pathology being investigated. This implies that we can now turn our attention to the more subtle problem of consistently distinguishing tissue types by means of their MRI signal characteristics. An increase in specificity may require a decrease in overall SNR; that is, imaging time may be more wisely spent increasing the specificity of the technique with the addition of different pulse sequences, rather than increasing the SNR by averaging the same pulse sequence. Any model of MRI should allow one to calculate the tradeoffs between overall SNR and specificity.

For the purpose of optimizing the application of MRI in the clinical environment we model it as an *in vivo* diagnostic test. When assessing the value of any diagnostic test, one must observe the distribution of test results obtained from the normal (those without the disease) and abnormal (those with the disease) patient populations. The performance of the test can be calculated by determining the overlap of these distributions.

2.1. Model of the Patient Population

It became evident quite early in the development of NMR in medicine that there was a large sample-to-sample variability in the measured values of T_1 and T_2 in the same tissue; this variability was much greater than the predicted error in the measurements (10-13). This does not come as a surprise; the medical community is quite familiar with the concept of the normal variant. Determination of optimal data acquisition protocols for differential diagnoses must incorporate this observed variability of tissue parameters (14). A single value for a tissue parameter does not adequately characterize a tissue; thus, statements such as “The T_1 of white matter is 700 ms at 1.5 T” are of limited worth.

The appropriate mathematical construct for modeling the variability of tissue parameter values found in a given tissue type is a probability density function (PDF). For MRI, a tissue specific probability density function (TPDF) describes the patient-to-patient variability of tissue parameters, and the variability within a single tissue in a single patient. A specific example will assist with the explanation of the TPDF and the underlying assumptions in its construction. Suppose that in each of 100 patients 10 separate volumes of interest in normal fibrous breast tissue are isolated with MRI, and two tissue parameters are measured in each volume. The resulting 1000 points are pairs of tissue parameter values, and as such may be plotted in a two-dimensional space. In this two-dimensional space the points will cluster together with a density described by the TPDF for normal fibrous breast. Such a two-dimensional distribution, based

NIH-PA Author Manuscript

NIH-PA Author Manuscript

NIH-PA Author Manuscript

on the tissue parameters T_1 and T_2, is shown in Fig. 1, accompanied by TPDFs for fat and infiltrating duct carcinoma (15). The extension to higher dimensions (more tissue parameters) is mathematically and conceptually straightforward.

There are a large number of tissue parameters that are now important in MRI: the relaxation times (before, after, and during the administration of contrast agents) T_1, T_2, $T_{1\rho}$, the proton density *N(H)*, the ratio of chemical species, the diffusion coefficient *D*, the magnetic susceptibility χ_0, and the velocity *v*, to name only the main ones. When collecting data to construct TPDFs, the number of tissue parameters measured in each voxel determines the dimension of the TPDF. Many of the tissue parameters are not mathematically independent, which increases the complexity of the TPDFs. This is discussed further in Section 4. In the following analysis it is assumed that the TPDFs are independent. If the tissue parameter values found in the lesion are correlated with those in the normal tissues, then the TPDFs as described here are inappropriate.

2.2. Model of the Imaging Data Acquisition

The relative signal strength values for most MRI pulse sequences and the effects of slice selection are predicted accurately by equations found in the literature (16-25). For the optimization procedure proposed here, we deliberately separate the tissue parameters, and the pulse sequence parameters. There is a fundamental difference between these two classes of variables; the tissue parameters are assumed to follow stationary TPDFs (they are the given in the diagnostic problem), while the pulse sequence parameters are the variables to be determined. The data collection process consists of transforming the entire tissue parameter space encompassed by the TPDFs into signal strengths. With this holistic model, we can investigate the interaction of the imager with a whole domain of possible tissue parameter values.

Mathematically, MRI data acquisition from the patient population is modeled by mapping the TPDFs from a tissue parameter space (*T*-space) to signal strength space (*S*-space). The transformed distributions can now be called signal probability density functions (SPDFs). The mapping comprises one or more signal strength equations, with the pulse sequence parameters fixed and the tissue parameters as independent variables; thus, each set of pulse sequence parameters produces an individual mapping with its domain in *T*-space and its range in *S*-space. Figure 2 shows how two Gaussian TPDFs (shown as 2σ perimeters) are mapped from a two-dimensional *T*-space into two SPDFs in a one-dimensional *S*-space.

In general, a mapping is given formally by

$$S_i = \psi_i\left(X_1, X_2, \cdots X_{N_p}; \mathrm{TR}, \mathrm{TE}, \mathrm{TI}, \alpha, \cdots\right) i = 1, 2, \cdots N_s, \quad [1]$$

where ψ_i is the signal strength function for each of the N_s pulse sequences used, and X_j are the tissue parameters, which are the independent variables in the expression. We see that N_p-dimensional points in the *T*-space (tissue) $(X_1, X_2, \ldots, X_{N_p})$ are mapped to N_s-dimensional points in the *S*-space (signal) $(S_1, S_2, \ldots, S_{N_s})$. In this manner, the TPDFs that give the expected distribution of tissue parameters, now give, as SPDFs, the distribution of expected signal values, which are the quantities that we measure during the MRI examination. Of course, the physical result of a mapping is a set of N_s images of a slice of the patient; these images comprise points in the *S*-space. The data acquisition optimization is simply the search for the best mapping, once a method of evaluating the efficacy has been established.

Modeling MRI data collection as shown in Fig. 2 makes one concept intuitively obvious. No mapping will improve the separation of the distributions; the SPDFs can only overlap as much or more than the TPDFs. Thus the separation of the TPDFs sets the upper bound on MRI as a

NIH-PA Author Manuscript

NIH-PA Author Manuscript

NIH-PA Author Manuscript

discriminator of tissues based on signal strength characteristics, regardless of the pulse sequences available. In Section 2.3 the quantitative evaluation of this separation is described.

An alternative method of visualizing how well a mapping will discriminate tissues is to look at isosignal contours for the individual pulse sequences in the *T*-space (26). If the *T*-space is of dimension N_p, the isosignal contours for a single pulse sequence, or an algebraic combination of pulse sequences, will be loci of dimension N_p - 1. Figure 3a shows an example of isosignal lines in the *T*-space for a single IR pulse sequence. In this case, the line $s = s_0$ acts as a good decision boundary between tissue A and tissue B. The representation of data collection shown in Fig. 3a demonstrates the cardinal idea underpinning this model of MRI; that is, *the signal strength equations provide us with discriminant functions in the T-space.* If one were modeling a diagnostic test, this concept would be taken for granted, but somehow in the development of MRI it seems to have been lost. This isosignal picture in *T*-space is useful for demonstrating how MRI will distinguish tissues, but when noise is included in the model the examination of the SPDFs in *S*-space becomes the simpler of the two pictures.

An essential part of any model of data acquisition is the behavior of the noise. The characteristics of the noise in spin-warp MR images are simple; the noise is spatially invariant, it has a flat power spectrum, and it follows a Gaussian PDF (27). Edelstein *et al.* (28) outlined a good SNR calibration procedure for MR imagers, which gives the SNR per milliliter times root hertz. Thus, given the minimum volume required for the diagnostic task, the bandwidth containing that volume, and the maximum signal strength obtainable from the imager, the expected root mean square deviation (RMSD) of the signal in the volume can be calculated. Thus, to incorporate noise into the model, each point in *S*-space is broadened by convolution with a Gaussian distribution whose breadth is the RMSD for the volume. After this convolution the overlap of the SPDFs will increase with the amount of the increase depending upon their proximity to one another. Extension to higher dimensions is straightforward. The changes in the noise level as a function of sampling and filtering have been described elsewhere (27,29, 30).

In this optimization procedure a number of imaging parameters are treated as constraints on the problem. These constraints are specified by the diagnostician and are task dependent. The minimum required resolution must be specified, that is, the dimensions of the smallest volume upon which the diagnostician expects to employ the diagnostic test. The total volume to be covered in the examination, the maximum imaging time, and the importance of artifact rejection must be specified as well. Assuming the constraints are not inconsistent, there will be a domain of possible pulse sequences and pulse sequence parameters from which the optimal mapping may be extracted.

2.3. Model of Performance Evaluation

When deriving a figure of merit, one must keep the diagnostic task in mind—to discriminate abnormal from normal tissues. The figure of merit should be an estimate of how well the technique performs this task. Performance estimates may be expressed in different forms, such as ROC curves (31), contingency tables (8), or risk functions calculated from Bayes' decision rule (32,33). The derivation of this type of figure of merit for the model described in Sections 2.1 and 2.2 is illustrated with an example in the following paragraph.

First, we deal with the calculation of the upper bound of performance. Suppose a clinical problem of interest has two tissues involved, normal tissue and a lesion. Suppose also that the two TPDFs for the tissues are known exactly for a two-dimensional *T*-space, say ($T_1 \times T_2$). In this example, the desire is to estimate how well we can distinguish each tissue from the other, without any assumption as to the cost of false identification. This means that we do not impose any external bias upon a decision rule; we let the TPDFs dictate how to classify a given point

NIH-PA Author Manuscript

NIH-PA Author Manuscript

NIH-PA Author Manuscript

in the $T_1 \times T_2$ plane. Because we make the assumption that the TPDFs are known exactly, this is a problem in statistical decision theory (32-34).

For the figure of merit, we require an estimate of how well separated the two tissues are with respect to their NMR characteristics. In order to evaluate the degree of separation, a decision rule must be constructed by which each point of the *T*-space is classified to be one of the two tissues. The rate of correct classification quantifies the degree of separation of the TPDFs. The decision rule for this example is simple; each point in the *T*-space will be classified as the tissue type whose TPDF has the greatest value at that point. In this way, two regions of the *T*-space are defined, one for each tissue. The decision boundary between these regions is the line on which the two TPDFs have equal value. This is illustrated in Fig. 4 for the TPDFs describing infiltrating duct carcinoma and fibrous breast tissue. This method of deriving a decision boundary can be applied to any set of TPDFs of known functional form.

The construction of the contingency table is simple for this example. The integral of the lesion TPDF on its side of the decision boundary will give the fraction of correct classifications of lesion. In this same region, the integral of the normal TPDF will give the probability of classifying the normal tissue as lesion. By repeating this process for the normal tissue one can calculate a 2×2 contingency table describing how accurately the MRI parameters discriminate these tissues and where the major confusions will arise. Extensions to more tissues is not difficult. This calculation will give the upper bound of the performance for any imaging technique that depends on the two tissue parameters chosen; therefore, one can hope to match but cannot exceed this performance with MRI data acquisition. This implies that, given unlimited examination time, one obtains the most accurate and specific examination by calculating the tissue parameters. However, this may not be the most efficient way of performing the diagnostic test, because we may be able to differentiate the tissues adequately with less information than is required to calculate the tissue parameters accurately.

In the example above, two important features have been omitted. These are the a priori probability that a disease will be present and the relative cost of the classification errors. First, let us deal with the a priori probabilities. The probability that a patient is bearing a lesion will depend on the population from which that patient is drawn. This a priori probability for the existence of a tissue is incorporated into the analysis by normalizing the TPDFs to reflect the prevalence of the tissue in the patient population. *This normalization will change the decision boundaries between tissues.* This aspect of the model is therefore important. The values used for the a priori probabilities will depend upon the clinical environment in which the MR scanner is being used.

The other factor that can influence the position of the decision boundaries is the relative cost of erroneous classifications. The radiologist's decision rule often varies with the situation. For example, if grave circumstances follow from a missed lesion (false-negative call), the radiologist will be more aggressive in calling cases positive. In contrast to this, if a positive call implies a morbid treatment regime with limited chance of cure, a more conservative call is appropriate. This variability in the threshold values for positive and negative calls can be built into the figure of merit through the use of a risk function (32).

Simply stated, the risk is the sum of the probabilities of all classifications, weighted by their respective costs. When this sum is a minimum, the optimum decision boundaries are found. The risk can be evaluated with the contingency table and a loss matrix, L_{ci}. The numerical values of the loss matrix are the relative cost associated with each element in the contingency table, that is, the loss associated with classifying tissue *i* as tissue *c*. For example, if L_{ci} were given as

		True tissue	

NIH-PA Author Manuscript

NIH-PA Author Manuscript

NIH-PA Author Manuscript

		$i = 1$	$i = 2$	$i = 3$
Classified tissue	$c = 1$	-2	2	2
	$c = 2$	1	-1	0
	$c = 3$	1	0	-1

this would imply a high reward for correctly identifying tissue 1 (negative cost), a high penalty for misclassifying tissues 2 or 3 as tissue 1, a moderate penalty for misclassifying tissue 1 as tissue 2 or 3, no penalty for confusing tissues 2 and 3 with each other, and moderate reward for correctly identifying tissues 2 or 3. If tissue 1 is considered the target, this loss matrix will weigh heavily against false-positive calls and more moderately against false-negative calls. The total risk for a given set of decision boundaries is calculated by multiplying each element of L_{ci} with its corresponding element in the contingency matrix, and then taking the sum of these products. The reader is referred elsewhere for a more detailed account of risk functions (32,33).

To estimate the actual performance obtained with MRI, the analysis is best done in the *S*-space. First, the TPDFs are mapped to the *S*-space. Second, the resulting SPDFs are convolved with the Gaussian noise function to give the final SPDFs that we expect to measure with the imager. Third, the same analysis that was applied to the TPDFs can be used to derive the contingency table and risk function representing the performance of the mapping. The optimization procedure is a search for the mapping that produces the risk that comes closest to that derived from the TPDFs.

3. An Example

Suppose we are presented with the simple problem of detecting a specific lesion in a background tissue. To derive the optimal MRI protocol for this task the following steps should be followed: (1) Characterize the lesion and the normal tissues found in the patient population as thoroughly as possible with TPDFs in a tissue parameter space. (2) Set the imaging constraints, such as maximum scan time, minimum resolution, minimum total volume scanned. (3) Decide upon an appropriate figure of merit for the task. (4) Search for the mapping (i.e., pulse sequence protocol) that produces the maximum figure of merit.

This process is illustrated for a hypothetical example in Fig. 5. In Fig. 5a two Gaussian distributions are plotted as 2σ contours in a two-dimensional *T*-space, $T_1 \times T_2$. They have the following parameters: tissue A, $\mu_{T_1} = 400$, $\sigma_{T_1} = 100$, $\mu_{T_2} = 40$, $\sigma_{T_2} = 10$, and a correlation coefficient $\rho = 0$; tissue B, $\mu_{T_1} = 600$, $\sigma_{T_1} = 100$, $\mu_{T_2} = 60$, $\sigma_{T_2} = 10$, and $\rho = 0$. In this example the a priori probabilities are the same and both distributions are normalized to unity; that is, the integral under the bivariate normal TPDF is 1.0. In Fig. 5b the two TPDFs are mapped into a one-dimensional *S*-space by an inversion recovery (IR) sequence with TR = 1100, TE = 35, and TI = 165. (This will be shown to be the optimal IR sequence.) The resulting SPDFs are convolved with a Gaussian model of image noise to produce the final SPDFs. The method of deriving this Gaussian was given in Section 2.3. For this example the imaging constraints were a total time of 5 min, a required resolution of 2 × 2 × 5 mm, 20 slices. The SNR at this resolution was assumed to be 100.

The figure of merit chosen is the minimum risk of the technique. Assuming equal cost for false-positive and false-negative calls, we define the risk as the sum of the false-positive rate and the false-negative rate. For each mapping a threshold signal s_0 is chosen in the *S*-space as a decision boundary. This divides the space into two domains: signals above s_0 will be called tissue A, signals below s_0 will be called tissue B. For a given value of the threshold signal s_0, a 2 × 2 contingency table is calculated and the risk evaluated. The set of all possible mappings and decision boundaries is searched for the minimum risk. The optimal mapping and decision boundary is shown in Fig. 5c.

NIH-PA Author Manuscript

NIH-PA Author Manuscript

NIH-PA Author Manuscript

The IR pulse sequence that produces the maximum SDNR between the *points* (600, 60) and (400, 40) in the $T_1 \times T_2$ plane, for the same imaging constraints, is TR = 1100, TE = 15, TI = 340. This is significantly different from the optimal IR pulse sequence derived from the risk calculation. In order to examine why this discrepancy occurs, it is instructive to look at plots of isosignal contours for each sequence in the $T_1 \times T_2$ plane. In Fig. 6a we show the SPDFs for the optimal sequence with the decision boundary marked on the axis. Corresponding to this, the two TPDFs are shown in the $T_1 \times T_2$ plane with the isosignal contours of the optimal sequence overlayed. The dashed isosignal contour serves as a good decision boundary for the TPDFs representing tissue A and tissue B. Figure 6b shows this same relationship between the SPDFs and the isosignal contours of the suboptimal sequence that produces the maximum SDNR between the points (600, 60) and (400, 40). Note that the overlap of the SPDFs is greater for this sequence than that for the optimal sequence of Fig. 6a. The reason for this is demonstrated well in the plot of isosignal contours for the suboptimal sequence shown in Fig. 6b. While the points (600, 60) and (400, 40) have the maximum SDNR in the suboptimal sequence of Fig. 6b, *there does not exist an isosignal contour that acts as a good decision boundary*. This demonstrates why it is important to model the tissues as TPDFs rather than discrete points.

One further point can be made with this simple example: in some instances, one can obtain close to maximum discrimination with far fewer data than are required to calculate the tissue parameters. Recall that the minimum risk one can obtain from *any* method that depends on T_1 and T_2 is calculated from the TPDFs in the *T*-space. For this example, the minimum risk calculated from the TPDFs is 0.1. This is close to that obtained with the single optimal sequence (in Fig. 6a 0.10 + 0.07 = 0.17).

4. Characteristics of the Model

In this section some conclusions regarding MRI data acquisition are drawn based on a mathematical analysis of this optimization procedure.

4.1. Dimensionality

For each clinical problem there are three fundamental quantities: the number of tissues involved (N_t), the number of parameters used to model these tissues (N_p), and the number of pulse sequences used in the protocol (N_s). Naturally, part of the optimization problem is to determine the most appropriate values for N_t, N_p, and N_s. The three dimensions are dependent upon one another. This section is devoted to investigating this dependence and how it affects the data acquisition philosophies.

The appropriate order of operations to determine the dimensions of the optimization problem is as follows.

1. Determine the number of tissues involved in the problem. For example, when looking for a lesion in the brain, one would include white matter, gray matter, CSF, and the lesion. This sets $N_t = 4$.
2. Decide whether one tissue will be treated as the target, or more than one tissue must be completely differentiated, and set the loss matrix accordingly. This may affect the number of both tissue parameters and pulse sequences needed.
3. Determine which tissue parameters offer the best potential in discriminating the target tissue from the background, or all tissues from each other. This sets the value of N_p.
4. Choose the pulse sequences used in the protocol as the mapping from *T*-space to *S*-space. This sets N_s.

NIH-PA Author Manuscript

NIH-PA Author Manuscript

NIH-PA Author Manuscript

4.1.1. Number of tissues, N_t—For a given radiological task, it is usually possible to name the tissues that will be involved. Attempting to find a lesion against a background of known normal tissues is a common case. If the number of tissues in the problem is N_t, including the lesion, there are N_t - 1 discrimination problems to consider. In the best case, one pulse sequence will supply all of the decision boundaries for the N_t - 1 discrimination problems. The other extreme situation has N_t tissues, all of which must be discriminated from each other, giving $N_t(N_t - 1)/2$ discrimination problems. For either of these situations, in order to be able to derive the best protocol, it is necessary to include all N_t tissues in the optimization simultaneously. Breaking the problem up into separate two-tissue problems may simplify the computational complexity, but the optimal solution may then not be obtained.

Most situations will lie between the two extreme cases of a single target tissue and a full N_t tissue discrimination problem. This character of the problem is modeled with the loss matrix, L_{ci} as described in Section 2.3.

4.1.2. Number of parameters, N_p—After deciding what tissues to include in the optimization, and their relative importance, one must choose which parameters should be used to model these tissues. This is an important step because the upper bound of the performance is set by the amount of overlap of the parameter values described by the TPDFs.

The amount of data needed to determine the TPDF function to within a specified accuracy increases exponentially with the dimension of the TPDF (32). This has come to be known as the curse of dimensionality (35). However, only a subset of the complete list of available parameters is usually needed to attack a given problem. In order to minimize expense, some a priori knowledge should be used when deciding to collect multivariate data for the purpose of characterizing tissues with TPDFs. The parameters chosen should not be highly correlated. If two parameters are highly correlated, one of them can usually be dropped without reducing the effective dimension of the *T*-space.

For each tissue parameter in the *T*-space, there must exist at least one pulse sequence which exploits differences in that parameter. This pulse sequence should be robust under the day-to-day variations in the operating conditions of the imager and be relatively simple to implement. Unless such a pulse sequence is devised, it may not be worth the effort to add the corresponding dimension to the TPDFs.

Addressing the problem of estimating PDF parameters or constructing parameter free PDFs from the collected data is beyond the scope of this paper. The theory for these processes is found in standard textbooks on pattern recognition and statistical decision theory (32-34). The bulk of published tissue parameter data cannot be used for fitting multiparametric PDFs. However, suitable data are starting to emerge (10-12,15). For the remainder of this paper it is assumed that the functional form of the TPDFs is known exactly. Optimization with incomplete knowledge of the functional form of the TPDFs will be treated in a subsequent paper.

4.1.3. Number of sequences, N_s—Data acquisition protocols can be divided into two classes of mappings: those that have the potential to be a one-to-one mapping and those that do not. In the first case a necessary condition is that the number of pulse sequences is greater than or equal to the number of tissue parameters in the pulse sequence equations, that is, $N_s \geq N_p$. In the second case, $N_s < N_p$. We deal with these cases separately.

In the context of this model of MRI data acquisition, $N_s < N_p$ implies that the mapping is many-to-one; i.e., it contracts the N_p-dimensional *T*-space to an N_s-dimensional *S*-space. Figure 3 shows a two-dimensional *T*-space ($N_p = 2$) being mapped to a one-dimensional *S*-space ($N_s = 1$) by an IR pulse sequence. Note that each point in the one-dimensional *S*-space corresponds

NIH-PA Author Manuscript

NIH-PA Author Manuscript

NIH-PA Author Manuscript

to a curve in the *T*-space. Therefore, the SPDF value at a point s_0 in the *S*-space corresponds to the line integral of the TPDF along the contour $s = s_0$ in the *T*-space. In Fig. 7 we show an example with $N_p = 3$, $N_s = 2$. In this case the isosignal contours for each sequence in the *T*-space are two-dimensional surfaces. The line of intersection of two surfaces, $S_1 = k_1$, $S_2 = k_2$, corresponds to a point in the *S*-space. Again, the value of the SPDF at the point (k_1, k_2) is the line integral of the TPDF in the *T*-space along the line of intersection of the two surfaces $S_1 = k_1$, $S_2 = k_2$.

In general, the contour surfaces of individual pulse sequences are $(N_p - 1)$-dimensional loci in the *T*-space. The intersections of the contour surfaces for the N_s sequences are loci of dimension $N_p - N_s$, and the SPDF value at a point in the *S*-space is the integral of the TPDF on this locus. In the special case of a one-sequence protocol ($N_s = 1$), one must pay special heed to the decision boundaries supplied by the pulse sequence isosignal contours in the *T*-space, for these are the only ones available. When N_s is greater than one, decision boundaries may be synthesized by algebraic combination of the images from each sequence.

In the alternative case when $N_s \geq N_p$, there exists the potential to construct a one-to-one mapping from the *T*-space to the *S*-space. This is equivalent to a coordinate transformation in the domain of the *T*-space for which the mapping is one-to-one. An example of this is given in Fig. 8 in which the "T_1-weighted, T_2-weighted" imaging protocol is shown mapping a domain of the $T_1 \times T_2$ plane ($N_p = 2$) to a range in the *S*-space; each point in the domain is uniquely defined by a pair of signal values. We can now construct *any* decision boundary we choose in this domain; therefore, the optimum decision boundary derived from the risk function and the TPDFs is available. This optimum decision boundary is, of course, mapped from the *T*-space to the *S*-space where it may be used directly; however, after the inclusion of noise it may no longer give optimal performance. When this happens, a new optimal decision boundary must be calculated from the SPDFs.

When the number of sequences is greater than the number of tissue parameters, the SPDFs are contained within an N_p-dimensional manifold in the N_s-dimensional *S*-space. In Fig. 9, for example, we assume that we have two pulse sequences ($N_s = 2$) which are dependent upon only one parameter, say T_2, and the *T*-space is one-dimensional. The mapping of the SPDFs in this case is from the one-dimensional T_2 axis to a curve in the two-dimensional signal strength plane. This situation is similar to that of a multiecho sequence. The pixels of an eight-echo sequence of images can be considered to be points in an eight-dimensional *S*-space. However, because the signal strength from echo to echo is only modulated by T_2, *most of this eight-dimensional space is empty.* In fact, if one normalizes out the T_1 and $N(H)$ dependence with the first image of the sequence (assuming TE $\ll T_2$), the pixels of the remaining seven normalized images lie near a single one-dimensional curve; excursions from this curve are due to image noise only. The relative position of the pixel on the curve is determined by the T_2 value of the voxel it represents.

The locus upon which the image data are contained in the *S*-space has a simple analytical expression. It is an N_p-dimensional manifold in the N_s-dimensional space, parameterized by the N_p tissue parameters. This relation is given by Eq. [1]. Thus, it is not surprising that when principal component analysis is performed on any number of pulse sequences which are dependent only on T_1 and T_2 ($N(H)$ and T_1 being highly correlated), nearly all of the information is contained in the first two components (36). In this case, the *T*-space is effectively two-dimensional and, therefore, the image information is mostly contained in a two-dimensional manifold contained in any *S*-space of dimension greater than two. (The first two PCA images are the basis of a *linear* manifold; therefore there will be some residual power in higher dimensions, but this is found to be small for the sequences used thus far.) One way of using the redundant images to advantage is to decrease the noise in the final displayed image. When

NIH-PA Author Manuscript

NIH-PA Author Manuscript

NIH-PA Author Manuscript

an *S*-space is contracted by combining images (for example, weighted addition of the multiecho images), the random noise level can be reduced with respect to the level of the coherent signal. The maximum gain in SNR available from this kind of contraction is $\sqrt{N}$ where N is the number of images used in the contraction.

5. Discussion

This paper has presented a new approach to optimizing MRI data acquisition protocols for differential diagnosis. The main innovation of the method is the movement away from the traditional methods of optimizing the imaging technology and toward the methods used for optimizing the diagnostic test. Two sources of previous work are useful in this study, those of statistical pattern recognition (32-34) and clinical decision analysis (9). The existing development of these theories is sufficiently general to apply them to MRI with few modifications.

One of the major drawbacks of this method of optimization is its dependence upon a data base to determine the TPDFs. There are two problems associated with acquiring these data: obtaining truth and the cost. In order to collect tissue parameter data from a specified tissue, one needs to unambiguously classify the tissue from which the data point is collected. This requires an independent method of classifying the tissue that has a very low probability of error. In MRI, the classification of the normal tissues can be done using anatomical location. For lesions the problem is more complicated, unless there are results from a biopsy or autopsy available. These difficulties magnify the importance of publishing tissue parameter data as correlated values from the same sample, not as independent means.

The imaging data that are collected using the optimal protocol offer the maximum separation between tissues in a mathematical sense. In order to translate this mathematical separation into a diagnostic improvement, a set of “display” images must be synthesized. The collected images can be considered a basis set from which display images are derived; the algorithm that synthesizes the display images may be changed according to the needs of the diagnostician. For example, it may be suitable to synthesize an image for each discrimination problem (i.e., lesion vs white matter, lesion vs gray matter).

The optimization algorithm described in this paper has mathematically separated tissue-dependent signal characteristics in the entire patient population; therefore, any image processing that is done automatically on all of the images should be based on the SPDFs. However, once the data for an individual have been taken, some image processing can be done based solely on the acquired data. Such processing includes principal component analysis (36,37), the calculation of eigenimages (38), and SDNR maximization between specific regions of interest (ROIs) with matched filters (39). For example, the radiologist may spot a region of suspicion in a background of normal tissue. By defining two ROIs, one for the region of suspicion, the other for the known normal tissue, the data in the *S*-space can be contracted by taking the sum of the collected images of the slice with weighting coefficients that produce maximum SDNR between the region of suspicion and the background. This summation is based on the data for *this patient only* and therefore may differ from that derived from the whole population. But, it should be noted that *the region of suspicion must be found first*; it is the job of the optimized protocol to give the radiologist the best chance at finding this region of suspicion. Once the region of suspcicion is found, many sophisticated image processing and data analysis techniques can be used.

NIH-PA Author Manuscript

NIH-PA Author Manuscript

NIH-PA Author Manuscript

6. Conclusions

A number of conclusions have been drawn throughout this analysis and are summarized for clarity in point form.

1. In order to derive the optimal data acquisition protocol, the natural variability of the tissue parameters must be taken into account.
2. The figure of merit needs to reflect the clinical task, not machine performance. For this reason the separability of tissues is a more pertinent figure of merit than SNR or SDNR.
3. The upper bound of separability of tissues with MRI signal values is set by the overlap of the PDFs describing the distribution of tissue parameter values in the patient population. The first stage of any optimization should be the calculation of the PDFs describing the tissue parameters.
4. All of the tissues relevant to the clinical problem must be included in the algorithm in order to derive the optimal protocol.
5. The prevalence of disease in the patient population can be accounted for through normalization of the TPDFs.
6. The relative importance of differentiating the tissues in the problem can be modeled with a loss matrix.
7. The effective dimension of the signal strength space is given by the number of tissue parameters upon which the pulse sequences are dependent. That is, all signal strength values will lie upon a manifold in a signal strength space whose dimension is determined by the number of tissue parameters (assuming the number of sequences is greater than or equal to the number of tissue parameters). Additional pulse sequences added to a protocol may stretch this manifold, but they will not increase its dimension unless a new, independent tissue parameter is introduced.
8. If the TPDFs are known exactly, the image extraction process used to derive the display images from the collected data can be established in advance. Further adaptive image processing may be done with human assistance based on what the radiologist finds in the display image set.

Acknowledgments

The authors thank Art Burgess, Adrian Crawley, and Patrick Goebel for their useful comments. This research was supported by the Medical Research Council, the National Cancer Institute of Canada, the Ontario Cancer Treatment and Research Foundation, the Ontario Ministry of Health, and Canadian General Electric Medical Systems. E. R. McVeigh was supported by the Ontario Ministry of Colleges and Universities.

References

1. Damadian R. Science 1971;171:1151. [PubMed: 5544870]
2. Edelstein WA, Bottomley PA, Hart HR, Smith LS. J. Comput. Assist. Tomogr 1983;7:391. [PubMed: 6841698]
3. Wehrli FW, MacFall JR, Glover GH, Grigsby N. Magn. Reson. Imaging 1984;2:3. [PubMed: 6530915]
4. Hendrick RE, Nelson TR, Hendee WR. Magn. Reson. Imaging 1984;2:193. [PubMed: 6530926]
5. Ortendahl DA, Hylton N, Kaufman L, Watts JC, Crooks LE, Mills CM, Stark DD. Radiology 1984;153:479. [PubMed: 6091173]
6. Young IR, Burl M, Bydder GM. J. Comput. Assist. Tomogr 1986;10:271. [PubMed: 3950156]
7. Buxton RB, Edelman RR, Rosen BR, Wismer GL, Brady TJ. J. Comput. Assist. Tomogr 1987;11:7. [PubMed: 3805431]

NIH-PA Author Manuscript

NIH-PA Author Manuscript

NIH-PA Author Manuscript

8. Weinstein, MC.; Fineberg, IV. Clinical Decision Analysis. Saunders; Philadelphia: 1980.
9. Droege RT, Wiener SN, Rzeszotarski MS. Radiology 1984;153:425. [PubMed: 6484175]
10. Henkelman RM, Hardy PA, Poon PY, Bronskill MJ. Radiology 1986;161:727. [PubMed: 3786723]
11. Herfkens R, Davis P, Crooks L, Kaufman L, et al. Radiology 1981;141:211. [PubMed: 7197379]
12. Davis P, Sheldon P, Kaufman L, Crooks L, Margulis AR, Miller T, Watts J, Arakawa J, Hoenninger J. Cancer 1983;51:433. [PubMed: 6821826]
13. Gordon R, Coumans J. Med. Phys 1983;11:79. [PubMed: 6700559]
14. Herbert DE. Magn. Reson. Imaging 1986;4:215. [PubMed: 3669933]
15. Bronskill, MJ.; Brown, DW.; Yaffe, MJ.; Johns, PC.; Foster, FS.; D'Astous, FT. Magnetic Resonance in Cancer. Pergamon; Toronto: 1986.
16. Ernst RR, Anderson WA. Rev. Sci. Instrum 1966;37:93.
17. Bakker CJG, De Graaf CN, van Dijk P. Phys. Med. Biol 1984;29:1511. [PubMed: 6514785]
18. van Uijen CMJ, den Boef JH. Magn. Reson. Imaging 1984;1:502.
19. Young IR, Bryant DJ, Payne JA. Magn. Reson. Med 1985;2:355. [PubMed: 4094552]
20. Hardy PA, Bronskill MJ, Henkelman RM. Med. Phys 1985;12:581. [PubMed: 2995779]
21. Sperber GE, Ericsson A, Hemmingsson A, Jung B, Thuomas KA. Magn. Reson. Imaging 1986;3:685.
22. Rosen BR, Pykett IL, Brady TJ. J. Comput. Assist. Tomogr 1984;8:195. [PubMed: 6323554]
23. Majumdar S, Orphanoudakis SC, Gmitro A, O'Donnell M, Gore J. Magn. Reson. Med 1986;3:397. [PubMed: 3724419]
24. Majumdar S, Orphanoudakis SC, Gmitro A, O'Donnell M, Gore J. Magn. Reson. Med 1986;3:562. [PubMed: 3747818]
25. Crawley AP, Henkelman RM. Magn. Reson. Med 1987;4:34. [PubMed: 3821477]
26. Kurtz D, Dwyer A. J. Comput. Assist. Tomogr 1984;8:819. [PubMed: 6470247]
27. McVeigh ER, Bronskill MJ, Henkelman RM. Med. Phys 1985;12:586. [PubMed: 4046992]
28. Edelstein WA, Bottomley PA, Pfeifer LM. Med. Phys 1984;11:180. [PubMed: 6727793]
29. Edelstein WA, Glover GH, Hardy CJ, Redington RW. Magn. Reson. Med 1986;3:604. [PubMed: 3747821]
30. Oppelt, A.; Stetter, E.; Loeffler, W. Soc. Magn. Reson. Med. First Annual Meeting; 1981; p. 121 [Abstract book]
31. Green, DM.; Swets, JA. Signal Detection Theory and Psychophysics. Krieger; Huntington, NY: 1973.
32. Meisel, WS. Computer Oriented Approaches to Pattern Recognition. Academic Press; New York: 1972.
33. Fukunaga, K. Introduction to Statistical Pattern Recognition. Academic Press; New York: 1972.
34. Duda, RO.; Hart, PE. Pattern Classification and Scene Analysis. Wiley; New York: 1973.
35. Bellman, RE. Adaptive Control Processes. Princeton Univ. Press; Princeton: 1961.
36. Smith, GD.; Mitchell, MR.; Pickens, DR.; Price, RR.; James, AE, Jr. Soc. Magn. Reson. Med. 5th Annual Meeting; 1986; p. 227[Abstract book]
37. Schmiedl U, Ortendahl DA, Mark AS, Berry I, Kaufman L. Magn. Reson. Med 1987;4:471. [PubMed: 3600253]
38. Miller JWV, Windham JP, Kwatra SC. IEEE Trans. Med. Imaging MI 1984;3:116.
39. Riederer SJ, Hall AL, Maier JK, Pelc NJ, Enzmann DR. Med. Phys 1983;10(2):209. [PubMed: 6346033]

NIH-PA Author Manuscript

NIH-PA Author Manuscript

NIH-PA Author Manuscript

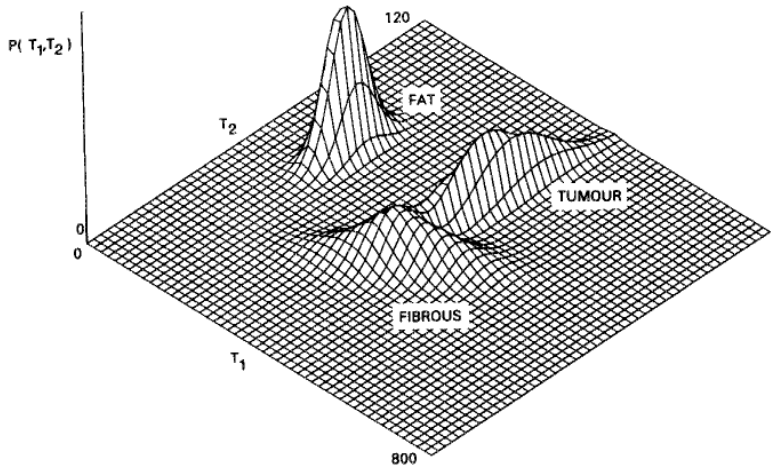

Fig. 1.

Three bivariate normal TPDFs in the $T_1 \times T_2$ plane. These distributions were derived from data measured *in vitro* for fat, fibrous, and infiltrating duct carcinoma tissues.

NIH-PA Author Manuscript

NIH-PA Author Manuscript

NIH-PA Author Manuscript

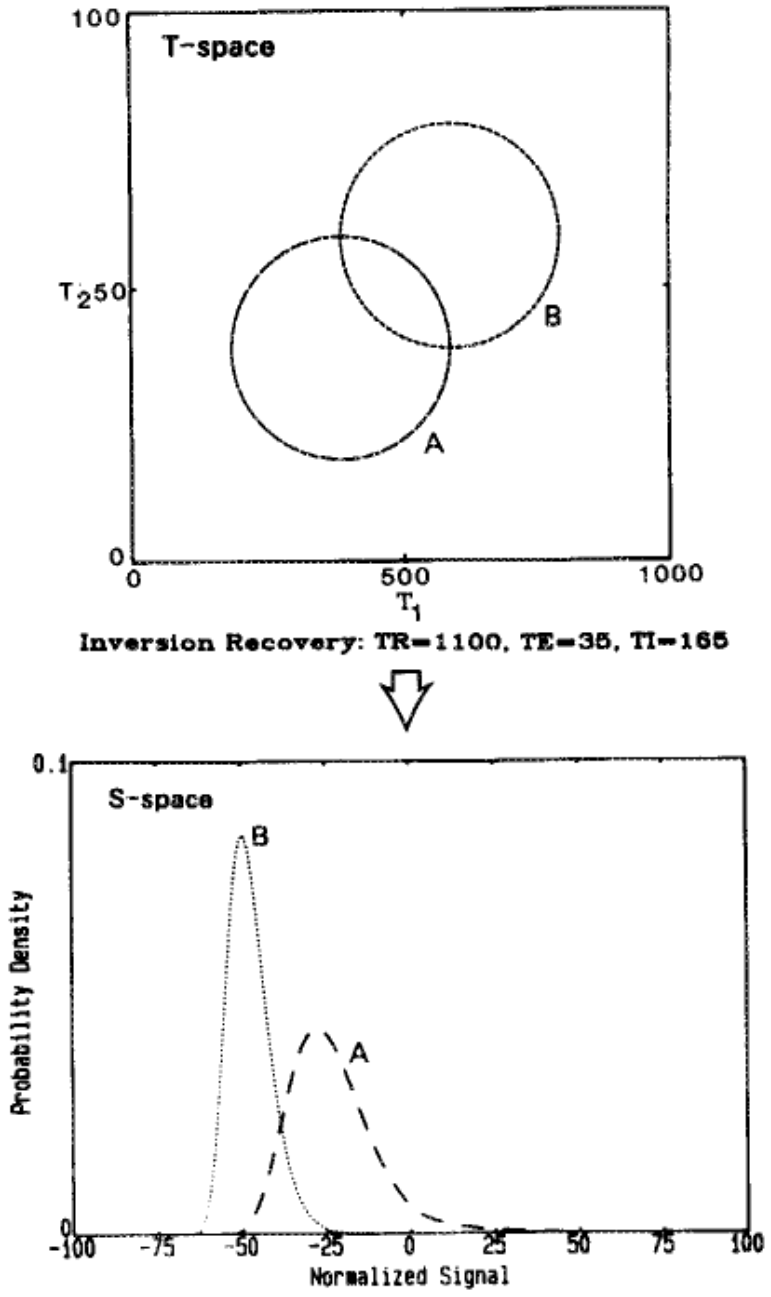

Fig. 2.

Two bivariate normal TPDFs with 2σ perimeters shown as dashed lines are mapped from a two-dimensional tissue parameter space (*T*-space) to a one-dimensional signal strength space (*S*-space) with an IR pulse sequence. The signal strengths are in units of the root mean square deviation (RMSD) of the image noise.

NIH-PA Author Manuscript

NIH-PA Author Manuscript

NIH-PA Author Manuscript

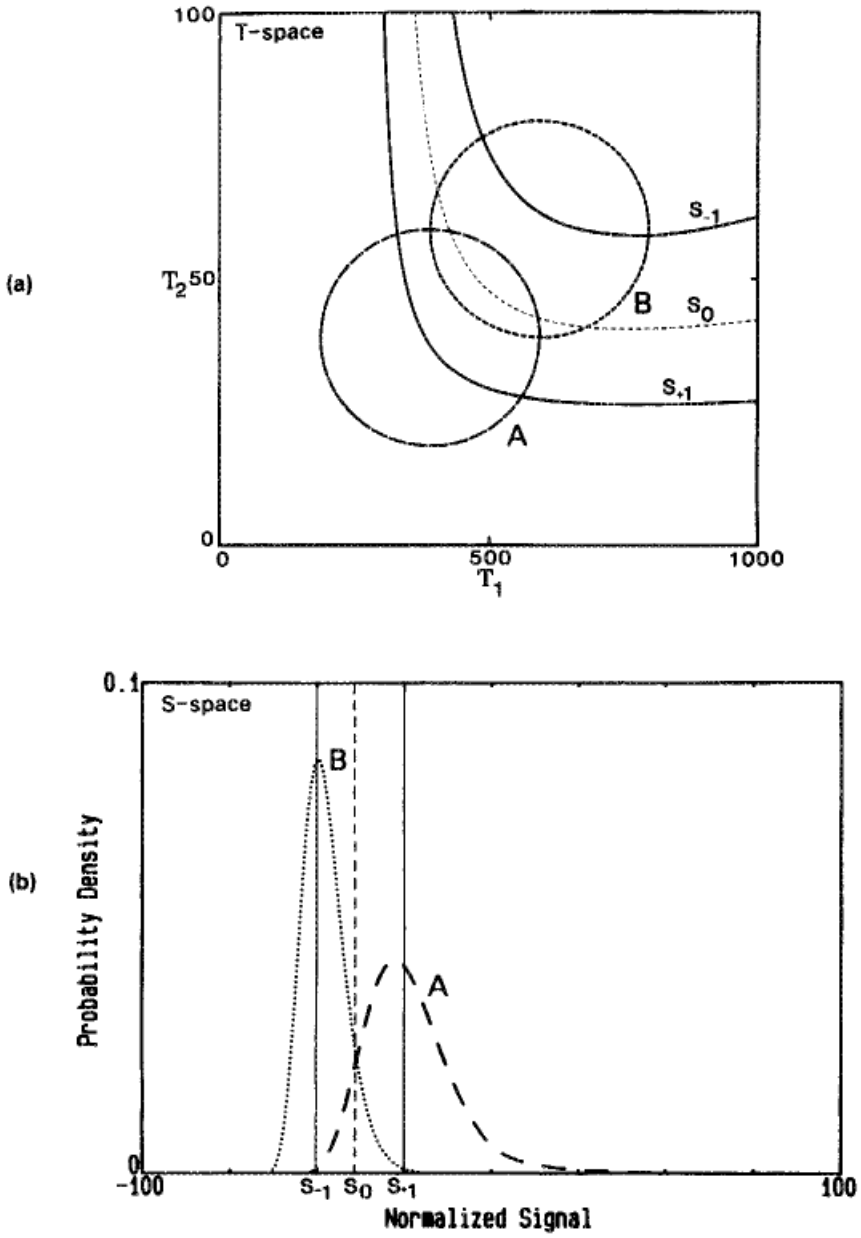

Fig. 3.

(a) Two bivariate normal distributions in *T*-space ($T_1 \times T_2$), with three isosignal contours from an IR pulse sequence overlayed. (b) Each contour maps to a single signal strength value as shown in the plot of the *S*-space. It is demonstrated in both the *T*-space and the *S*-space that the signal value $s = s_0$ acts as a good decision boundary between tissue A and tissue B.

NIH-PA Author Manuscript

NIH-PA Author Manuscript

NIH-PA Author Manuscript

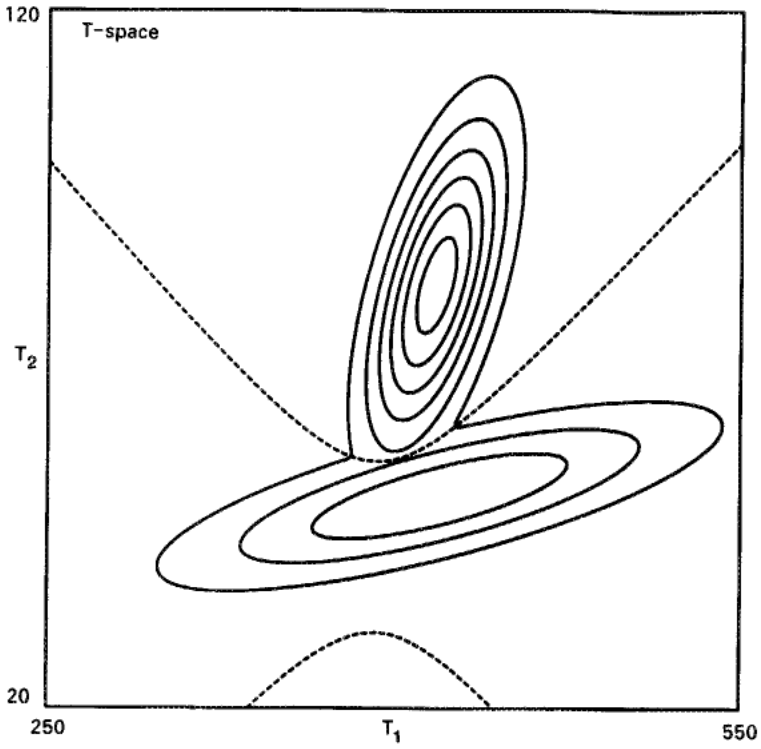

Fig. 4.
TPDFs for fibrous breast tissue (bottom) and infiltrating duct carcinoma (top) are shown as isoprobability density contours. The dashed line is the decision boundary derived from these TPDFs when the costs of both types of error (false-positive and false-negative) are identical.

NIH-PA Author Manuscript

NIH-PA Author Manuscript

NIH-PA Author Manuscript

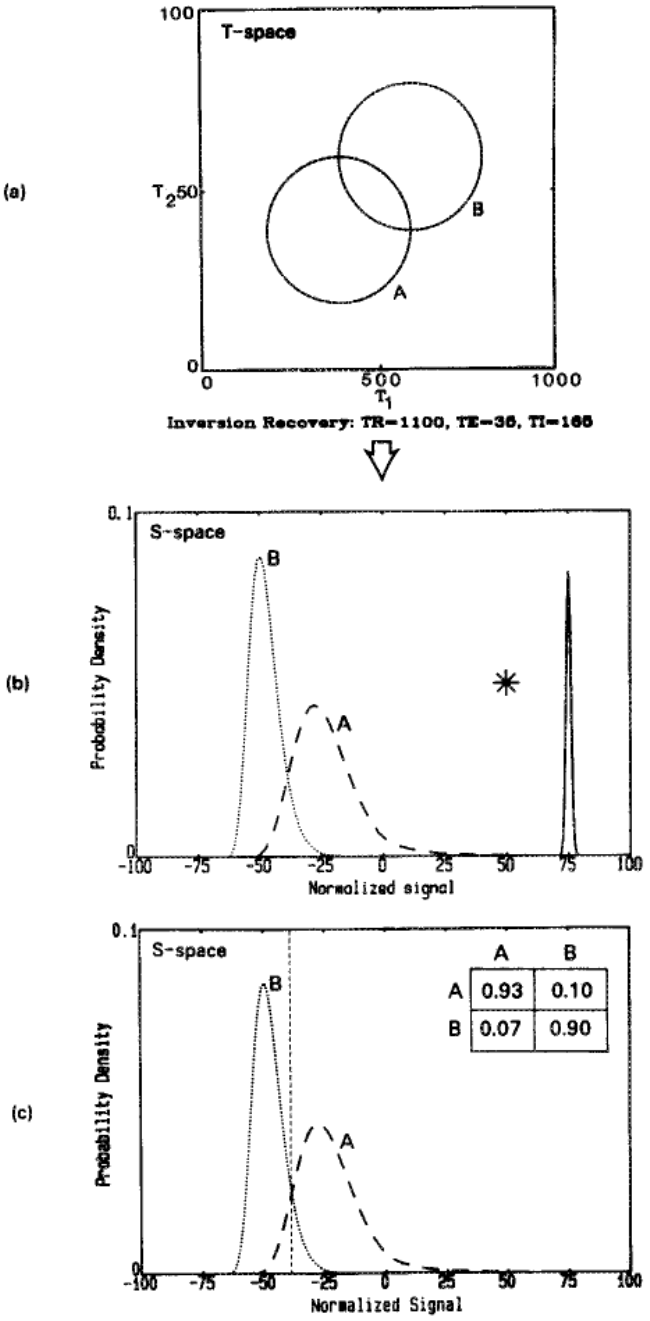

Fig. 5.

The method of optimization shown in three steps. (a) The model of the tissues. (b) The mapping to an *S*-space and the incorporation of image noise. (Note: the Gaussian is scaled down for display purposes.) (c) Selection of the decision boundary and risk calculation.

NIH-PA Author Manuscript
NIH-PA Author Manuscript
NIH-PA Author Manuscript

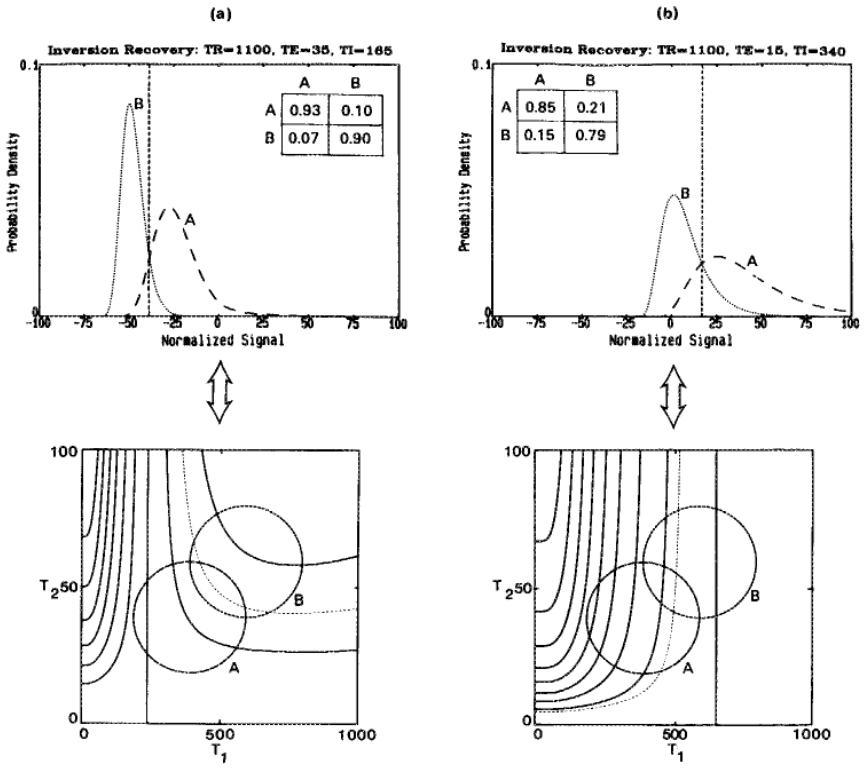

Fig. 6.

The SPDFs and associated TPDFs for two sequences. The TPDFs have isosignal contours of the sequence overlayed. The sequence shown in (a) has the minimum risk, the sequence in (b) has the maximum SDNR between the means of the TPDFs. Note the poor decision boundaries provided by sequence (b).

NIH-PA Author Manuscript

NIH-PA Author Manuscript

NIH-PA Author Manuscript

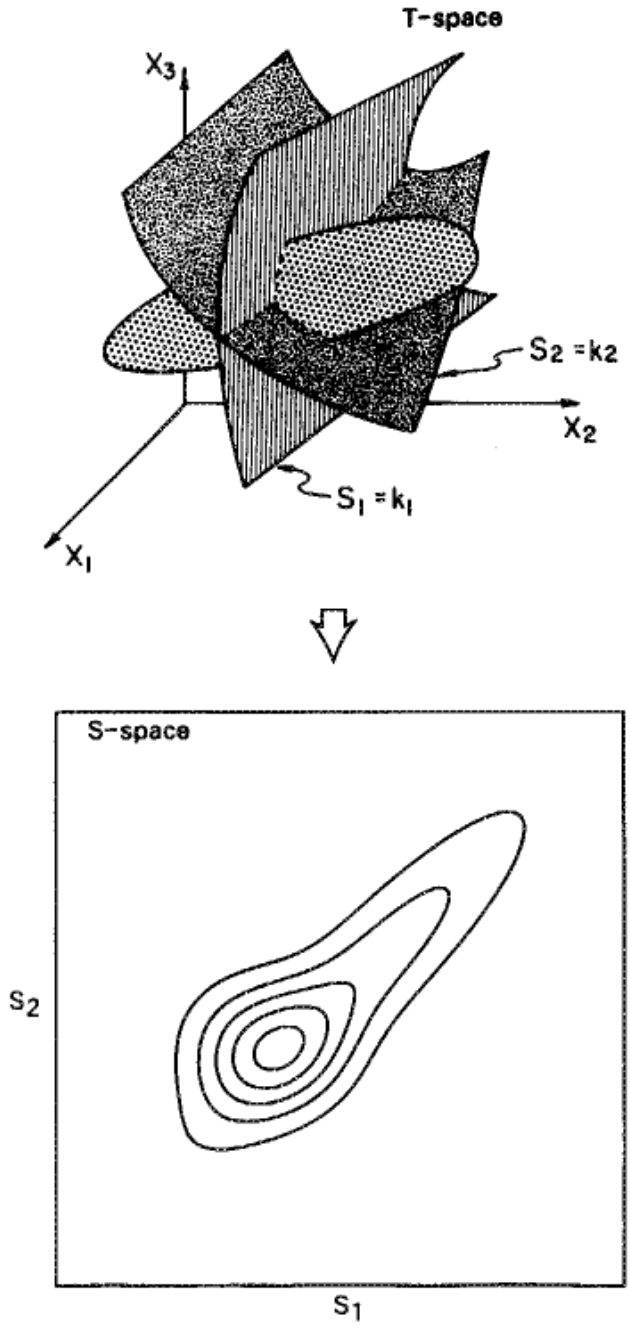

Fig. 7.

A schematic of a mapping for which $N_s < N_p$. In this case the mapping is from a three-dimensional *T*-space to a two-dimensional *S*-space. The TPDF is shown as an ellipsoid with isosignal surfaces intersecting it. One isosignal surface from each pulse sequence is shown. The integral of the TPDF along the line of intersection of the two surfaces gives the value of the SPDF at a point in the two-dimensional *S*-space. The SPDF is shown as isoprobability density contours in the *S*-space.

NIH-PA Author Manuscript

NIH-PA Author Manuscript

NIH-PA Author Manuscript

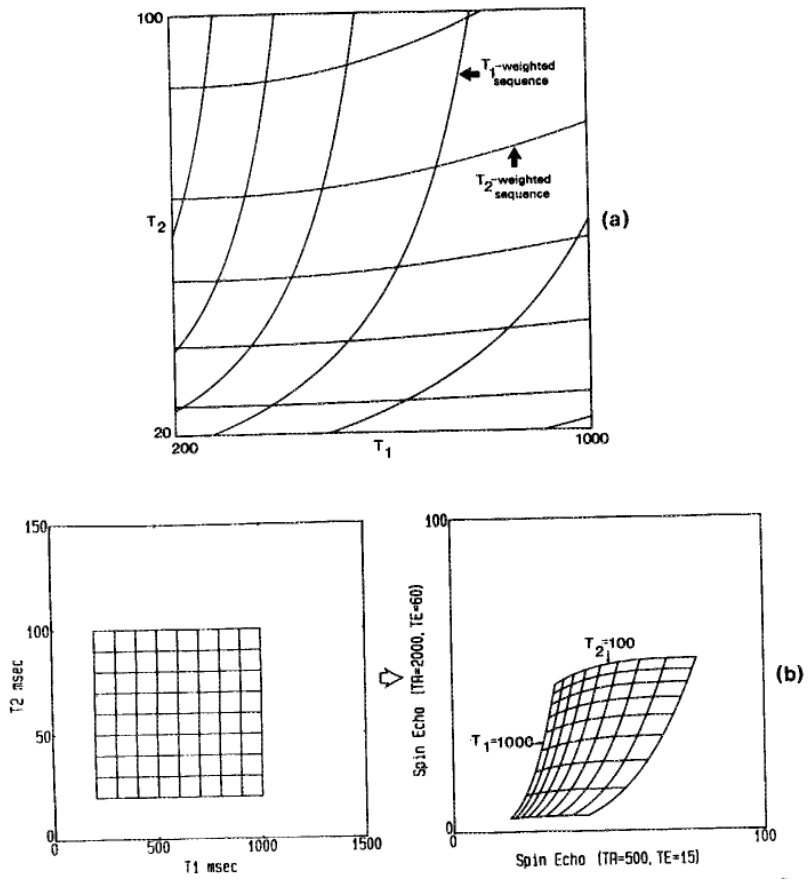

Fig. 8.

A one-to-one mapping from a two-dimensional *T*-space ($T_1 \times T_2$) to a two-dimensional *S*-space (spin-echo, T_1-weighted × T_2-weighted). (a) The isosignal contours draw a grid over a region in the *T*-space. (b) The same region of *T*-space as that in (a) mapped into the *S*-space. The grid shown in the *S*-space is equivalent to a set of curvilinear coordinates.

NIH-PA Author Manuscript

NIH-PA Author Manuscript

NIH-PA Author Manuscript

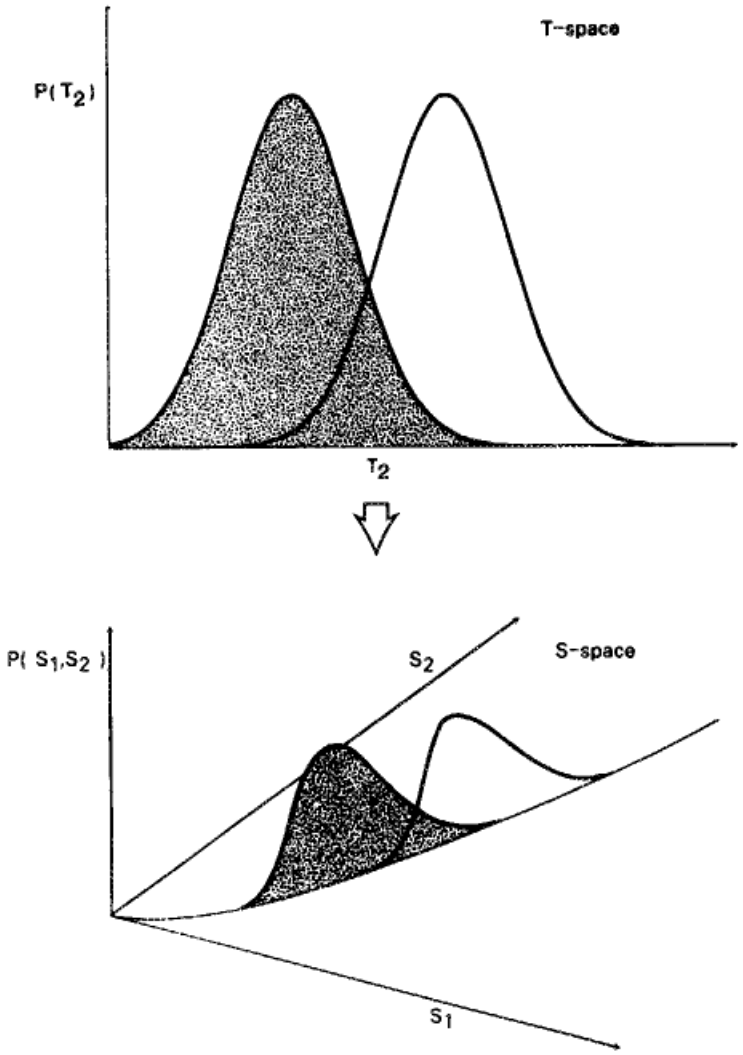

Fig. 9.

A mapping for which $N_s > N_p$. In this case the mapping is from a one-dimensional *T*-space (T_2) to a two-dimensional *S*-space (spin-echo, TE = *k*, TE = 3*k*). Note that all of the signal strenghts will be confined to the curve $S_2 = S_1^3$.